BUILDING RESEARCH JOURNAL
VOLUME 60, 2012 NUMBER 3 – 4

MESH-FREE FORMULATIONS FOR SOLUTION OF BENDING PROBLEMS FOR THIN ELASTIC PLATES WITH VARIABLE BENDING STIFFNESS. PART II: NUMERICAL SOLUTIONS

LADISLAV SATOR, VLADIMIR SLADEK AND JAN SLADEK

The second part of the paper is devoted to the development of mesh-free computational methods and numerical solutions of boundary value problems for thin plate bending problems treated in Part I within the Kirchhoff-Love theory. The in-plane gradation of the Young modulus and/or the variability of the plate thickness lead to governing equations which are the partial differential equations with variable coefficients. On the other hand, the transversal gradation of the Young modulus gives rise to coupling between the deflections and in-plane deformations. To facilitate the numerical solution of the boundary value problems for such rather complex governing equations, we propose the strong formulation combined with meshless approximations for field variables. Two alternative meshless approximation schemes are employed: the Moving Least Square (MLS) approximation and the Point Interpolation Method (PIM). The modified differentiation is proposed to increase the accuracy of higher order derivatives of field variables. Several numerical examples are presented to investigate the accuracy, convergence of accuracy and computational efficiency of studied mesh-free formulations for various boundary value problems for circular plate with central hole and variable bending stiffness.

Keywords: Kirchhoff-Love theory, variable thickness, functionally graded materials, decomposed formulation, strong formulation, meshless approximations

1. Introduction

Due to the great potential in engineering applications, the functionally graded materials (FGM) are in the focus of researchers. FGM structure can be characterized as a composite fabricated by mixing two discrete phases of materials (Suresh and Mortensen, 1998; Koizumi, 1997). The effective material properties, such as Young's modulus, Poisson's ratio, mass density, etc. of the functionally graded composites are being evaluated based only on the volume fraction distribution of the dispersed phases, because the accurate information of the distribution of constituents may not be available. In the literature several approaches are available for FGM modelling, like Mori – Tanaka scheme (Mori and Tanaka, 1973; Benveniste, 1987), composite cylindrical assemblage model (Hashin and Rosen, 1964; Hashin, 1979), the simplified strength of materials method (Chamis and Sendeckyj, 1968; Gibson, 1994), etc.

Institute of Construction and Architecture, Slovak Academy of Sciences, Dubravska cesta 9, 845 03 Bratislava 45, Slovak Republic, e-mail: ladislav.sator@savba.sk, vladimir.sladek@savba.sk, jan.sladek@savba.sk

Although FGMs are highly non-homogeneous structures, it will be very useful to idealize them as continua with their mechanical properties changing smoothly with respect to the spatial coordinates. Exact solutions of boundary value problems in solid mechanics can be obtained by this idealization and also it will help in developing numerical models of the structures made of FGMs (Sladek and Sladek, 2010; Sladek, Sladek and Sator, 2013). The static behaviour of FG rectangular plates was studied by Reddy (Reddy, 2000), and also an axi-symmetric formulation for circular and annular FG plate bending was observed (Reddy, Wang and Kitipornchai, 1999) within the 3rd order shear deformation plate theory. Xu and Zhou (Zhoua, 2009) studied rectangular FG plates with variable plate thickness and exponential gradation of Young's modulus in lateral direction as a 3D problem.

In recent two decades, the mesh-free formulations have become an attractive alternative of classical mesh-based discretization methods (such as FEM, BEM, etc.) because of various advantages (Atluri, 2004) resulting from the fact that only nodes are used for approximation instead of elements and no elements are needed either for background integration like in the Element Free Galerkin method (Krysl and Belytschko, 1995; Lu, Belytschko and Gu, 1994). Additional advantages of the mesh-free formulations arise in numerical solutions of boundary value problems for partial differential equations (PDE) with variable coefficients like in the case of functionally graded materials (FGM), since the complexity is not increased as compared with the case of homogeneous media. On the other hand, in the standard FEM the material coefficients are assumed to be constant within the finite elements, and in the BEM the fundamental solutions for the PDE with variable coefficients are not available, in general.

The main criticism against meshless approximations is the loss of accuracy and computational efficiency with increasing the order of the derivatives needed in mesh-free formulations. These shortcomings of the mesh-free formulation for thin plate bending problems have been removed in the Part I of this paper by developing the decomposed formulation. Two meshless approximations are employed in numerical implementations: (i) the Point Interpolation Method (PIM) with using radial Basis Functions (RBF) in combination with polynomials (Liu, 2003; Sladek, Sladek and Tanaka, 2005); (ii) the Moving Least Square (MLS) approximation (Lancaster and Salkauskas, 1981) with using the so called Central Approximation Node (CAN) concept (Sladek, Sladek and Ch. Zhang, 2008). As regards the numerical evaluation of the derivatives of field variables, we shall use the standard as well as the modified differentiation (Sladek and Sladek, 2010; Sladek, Sladek and Sator, 2013; Suresh and Mortensen, 1998) with focusing on numerical tests for accuracy and computational efficiency of these approaches. Moreover, the modified evaluation of the shape functions and their derivatives will be employed (Sladek and Sladek, 2010; Sladek, Sladek and Sator, 2013; Suresh and Mortensen, 1998) in order to obey correctly the requirements of completeness. The accuracy and convergence study is accomplished on boundary value problems for bending of thin circular plate with a central circular hole, where the exact solutions are available and can be used as the benchmark solutions. The power-law gradation of the bending stiffness along the radius as well as the transversal gradation of the Young modulus have been assumed in these studies.

The attention is paid also to numerical parametric study with respect to various parameters of gradations of the Young modulus and the thickness of the plate. The competitive influence of radial gradations of the Young modulus and the variable plate thickness is observed and it can be utilized in optimization design of plates.

2. Formulation of analyzed boundary value problems

In the Kirchhoff-Love theory, the bending of thin elastic plates is described by displacements specified at the mid-plane of the plate as functions of the in-plane coordinates. Moreover, mostly

there is no coupling between the transversal displacement (deflection of the plate) and the in-plane components of displacements. In the case of FGM plates with transversal gradation of the Young modulus, however, such a coupling plays an important role. In this paper, we confine to axially symmetric bending problems for circular and/or annular plates. Bearing in mind the results of the analysis presented in [Part I], we can write the governing equations for the plate with transversally graded Young modulus (while homogeneous in radial direction and with constant thickness) as

$$\frac{\omega_p L}{h_0}\left(\partial_r^2 u_r^* + \frac{1}{r}\partial_r u_r^* - \frac{1}{r^2}u_r^*\right) + \frac{c\zeta s_p}{D_V^*}\partial_r m^* = 0 \tag{1}$$

$$D^*\nabla^2 w^* + m^* = 0 \tag{2}$$

$$\nabla^2 m^* = -\frac{H}{(1-\nu)F}\lambda_0^* \tag{3}$$

where $u_r^*(r)$ and $w^*(r)$ are the radial displacement and deflection, respectively, while $m^*(r)$ is the new field variable defined by Eq.(2). Introduction of this new variable enables us decompose the original 4th order PDE into two Poisson equations. The superscript star is used for dimensionless quantities defined in [Part I] (for radial coordinate this superscript is omitted for conciseness). The dimensionless loading λ_0^* is assumed to be a uniform transversal loading. Remember the meaning or the definitions of the coefficients appearing in Eqs. (1) – (3):

- ζ is the level of transversal gradation of the Young modulus according to the power-law:
  $E = E(\mathbf{x}, x_3) = E_0 E^V(x_3) E^H(\mathbf{x})$, $E^V(x_3) = 1 + \zeta\left(\frac{1}{2} + \frac{x_3}{h}\right)^p$, ($E^H(\mathbf{x}) = 0$ in this case)
- bending stiffness: $D_0 D_V^* D_H^*(\mathbf{x})$, $D_0 = \frac{E_0 (h_0)^3}{12(1-\nu^2)}$, $D_V^* := \beta_p - 12\frac{(c\zeta s_p)^2}{\omega_p}$, $D_H^*(\mathbf{x}) := E^H(\mathbf{x})\left(h^*(\mathbf{x})\right)^3$
- plate thickness: $h = h_0 h^*$, h_0 – reference thickness, h^* – dimensionless thickness ($h^* = 1$ in this case)
- characteristic lateral dimension: $L = r_1 - r_0$, where r_1, r_0 are outer and inner radii of plate
- $s_p := \frac{1}{p+2} - \frac{1}{2(p+1)}$, $f_p := \frac{12}{p+3} - \frac{12}{p+2} + \frac{3}{p+1}$, $\omega_p := 1 + \frac{\zeta}{p+1}$
- $H = \begin{cases} 1-\nu, & \text{for plane stress states} \\ 1-2\nu, & \text{otherwise} \end{cases}$, $F = H + \nu$

Another considered case is the plate whose Young modulus is not graded across the plate thickness, i.e. when $\zeta = 0$, but the thickness and the Young modulus are allowed to be variable in the radial direction. Then, the deflections and radial displacements are decoupled with the governing equations for the bending being given as

$$D^*\nabla^2 w^* + m^* = 0, \qquad D^*(\mathbf{x}^*) = D_H^*(\mathbf{x}^*) = E_H(\mathbf{x}^*)\left(h^*(\mathbf{x}^*)\right)^3, \qquad D_V^* = 1 \tag{4}$$

$$\nabla^2 m^* - \frac{H}{FD^* r}\left(\partial_r D^*\right)m^* - \frac{H}{Fr}\left(\frac{1}{r}\partial_r D^* - \partial_r^2 D^*\right)\partial_r w^* = -\frac{H}{(1-\nu)F}\lambda_0^* \tag{5}$$

Recall that in this case $H = 1 - \nu$, $F = 1$, because $\zeta = 0$ justifies application of the plane stress formulation (there is no coupling).

The relevant quantities for specification of boundary conditions on boundary edges are: deflection (w^*), normal slope ($\partial w^* / \partial \mathbf{n}$), bending moment ($M^*$), generalized shear force (V^*), radial displacement (u_r^*), in-plane tractions (T_r^*) with all of them being expressed in terms of primary fields (w^*, m^*, u_r^*) and their derivatives as:

$$T_r^* = \pm 12 \frac{1-\nu}{H} \frac{\omega_p L}{h_0 D_V^*} \left\{ \frac{D^*}{h^{*2}} \left(F \frac{\partial}{\partial r} + \frac{\nu}{r} \right) u_r^* + \frac{\gamma_p}{h^*} \left(F m^* + \frac{H D^*}{r} \frac{\partial w^*}{\partial r} \right) \right\}, \tag{6}$$

$$M^* = n_\alpha n_\beta M_{\alpha\beta}^* = \frac{1-\nu}{H} \frac{\beta_p}{D_V^*} \left(F m^* + \frac{D^* H}{r} \partial_r w^* \right) + \frac{1-\nu}{H} \alpha_p \frac{D^*}{h^* D_V^*} \left(F \partial_r + \frac{\nu}{r} \right) u_r^* , \tag{7}$$

$$\begin{aligned} V^* = n_\alpha M_{\alpha\beta,\beta}^* + \frac{\partial T^*}{\partial \mathbf{t}} = n_\alpha M_{\alpha\beta,\beta}^* = \pm (1-\nu) \left(\frac{F}{H} \partial_r m^* - \frac{\partial_r D^*}{r} \partial_r w^* \right) + \\ \pm \frac{1-\nu}{H} \frac{\alpha_p \gamma_p}{D_V^*} \frac{\partial_r h^*}{h^*} \left(F m^* + \frac{H D^*}{r} \partial_r w^* \right) \pm \frac{1-\nu}{H} \frac{\alpha_p D^*}{D_V^*} \frac{\partial_r h^*}{(h^*)^2} \left(F \partial_r + \frac{\nu}{r} \right) u_r^* , \end{aligned} \tag{8}$$

where $\alpha_p = 12 \frac{c \zeta s_p L}{h_0}$, $\gamma_p := \frac{c \zeta s_p h_0}{\omega_p L}$. (9)

Usually, we need the expressions for M^* and V^* on the simply supported and/or free edges, where these quantities are prescribed. On such edges, however, the in-plane tractions vanish [$T_{\alpha\beta}^* n_\beta = 0$ in Eq. (6)] and the expressions for the bending moment and the generalized shear force can be

$$M^* = (1-\nu) \left[\frac{D^*}{r} \frac{\partial w^*}{\partial r} + \frac{F}{H} m^* \right], \tag{10}$$

$$V^* = \pm (1-\nu) \left(\frac{F}{H} \partial_r m^* + \frac{\partial_r D^*}{r} \partial_r w^* \right). \tag{11}$$

Note that the relevant boundary quantities do not involve higher than the first order derivatives of the primary field variables.

Physically correct boundary conditions result from the imperative satisfaction of the conditions:

$$n_\beta T_{\alpha\beta} \delta u_\alpha = 0 , \quad M \delta \left(\frac{\partial w}{\partial \mathbf{n}} \right) = 0 , \quad V \delta w = 0. \tag{12}$$

Three basic boundary conditions on a boundary edge Γ are known as

- clamped edge: $w|_\Gamma = 0$, $\left.\frac{\partial w}{\partial n}\right|_\Gamma = 0$
- simply supported edge: $w|_\Gamma = 0$, $M|_\Gamma = 0$
- free edge: $M|_\Gamma = 0$, $V|_\Gamma = 0$

3. Meshless approximation techniques

Two kinds of meshless approximations will be described shortly. For the sake of brevity, we shall use the common notation $u(\mathbf{x})$ for the scalar fields $w(\mathbf{x})$, $m(\mathbf{x})$ and the radial component of displacements $u_r^*(r)$. The nodal points are freely distributed in the analyzed domain and on its boundary without creating any connectivity among the nodes. Then, the approximated field is expressed in terms of certain nodal values and shape functions, which are not given by simple interpolation polynomials but certain procedure is required for calculation of their values at field points.

Moving Least Square (MLS) approximation

In the MLS-approximation, the polynomial basis $\{p_\mu(\mathbf{x})\}_{\mu=1}^m$ is employed and the expansion coefficients are found from minimization of weighted squares of residua at a finite number of nodal points (Gu and Liu, 2001). Finally, the scalar field $u(\mathbf{x})$ can be approximated as

$$u(\mathbf{x}) \approx \sum_{a=1}^{N} \hat{u}^a \phi^a(\mathbf{x}) \quad , \tag{13}$$

where N is the total number of nodes, $\hat{u}^a$ is a nodal unknown different from the nodal value $u(\mathbf{x}^a)$, and $\phi^a(\mathbf{x})$ is the shape function associated with the nodal point $\mathbf{x}^a$. Instead of the standard MLS--approximation, one can utilize the Central Approximation Node (CAN) concept of the MLS--approximation (Sladek, Sladek and Zhang, 2008). Let $\mathbf{x}^q$ be the CAN for the approximation at a point $\mathbf{x}$. Then, the amount of nodes involved into the approximation at $\mathbf{x}$ is reduced a-priori from N to N^q, where N^q is the number of nodes supporting the approximation at the CAN $\mathbf{x}^q$, i.e. the amount of nodes in the set $M^q = \left\{\forall \mathbf{x}^a;\, w^a(\mathbf{x}^q) > 0\right\}_{a=1}^N$, where $w^a(\mathbf{x})$ is the weight function associated with the node $\mathbf{x}^a$ and taken at the field point $\mathbf{x}$. In this paper, we employ the Gaussian weights (Sladek, Sladek and Zhang, 2008). The MLS-CAN approximation is given as

$$u(\mathbf{x}) \approx \sum_{a=1}^{N^q} \hat{u}^{\bar{a}} \phi^{(q,a)}(\mathbf{x}) \quad , \quad \bar{a} = n(q,a) \tag{14}$$

where $\bar{a}$ is the global number of the a-th node from the N^q nodal points $\mathbf{x}^{\bar{a}} \in M^q$. The CAN node can be selected as the nearest node to the field point $\mathbf{x}$.

The derivatives of the field variable $u(\mathbf{x})$ can be approximated in a standard way by differentiating the approximation (14), i.e.

$$u_{,i}(\mathbf{x}) \approx \sum_{a=1}^{N^q} \hat{u}^{\overline{a}} \phi_{,i}^{(q,a)}(\mathbf{x}), \quad u_{,ij}(\mathbf{x}) \approx \sum_{a=1}^{N^q} \hat{u}^{\overline{a}} \phi_{,ij}^{(q,a)}(\mathbf{x}), \quad u_{,ijk}(\mathbf{x}) \approx \sum_{a=1}^{N^q} \hat{u}^{\overline{a}} \phi_{,ijk}^{(q,a)}(\mathbf{x}), \tag{15}$$

The shape functions and their derivatives are given in Sladek, Sladek and Zhang (2008).

Point interpolation method (RBF+P)

In the case of PIM, the basis functions are taken as a combination of polynomials and radial basis functions (RBF) (Liu, 2003). Thus, one can solve the problem of accuracy and numerical stability of the approximation (Liu, 2003; Sladek, Sladek and Zhang, 2008). In this paper, we shall consider the same polynomial basis as in the MLS-approximation and the RBFs will be taken as multiquadrics

$$R^n(\mathbf{x}) = \left(\left| \mathbf{x} - \mathbf{x}^n \right|^2 + (c^n)^2 \right)^{\mu/2}, \tag{15}$$

with c^n being the shape parameter.

The approximation of the field variable $u(\mathbf{x})$ can be expressed by

$$u(\mathbf{x}) \approx \sum_{a=1}^{N^q} u^{\overline{a}} \varphi^{(q,a)}(\mathbf{x}), \quad \overline{a} = n(q,a), \tag{16}$$

i.e. formally, it is the same as in the MLS-approximation, but now the nodal unknowns are directly the values of the approximated field variable, since the shape functions obey the Kronecker – delta property $\varphi^{(q,a)}(\mathbf{x}^b) = \delta_{ab}$. This difference is substantial (e.g. for the development of the modified scheme for calculation of derivatives of field variables), as it will be seen later.

In standard differentiation-approach, the derivatives of the field variable are given as

$$u_{,i}(\mathbf{x}) \approx \sum_{a=1}^{N^q} u^{\overline{a}} \varphi_{,i}^{(q,a)}(\mathbf{x}), \quad u_{,ij}(\mathbf{x}) \approx \sum_{a=1}^{N^q} u^{\overline{a}} \varphi_{,ij}^{(q,a)}(\mathbf{x}), \quad u_{,ijk}(\mathbf{x}) \approx \sum_{a=1}^{N^q} u^{\overline{a}} \varphi_{,ijk}^{(q,a)}(\mathbf{x}), \tag{17}$$

with the shape functions and their derivatives being given in Sladek, Sladek and Tanaka (2005).

3.1 Modified shape functions

It is worth considering the modification of shape functions and their derivatives. Using the definitions (Sladek, Sladek and Sator, 2013)

$$s(\mathbf{x}) := \sum_{a=1}^{N^q} \phi^{(q,a)}(\mathbf{x}), \quad s_i(\mathbf{x}) := \sum_{a=1}^{N^q} \phi_{,i}^{(q,a)}(\mathbf{x}), \quad s_{ij}(\mathbf{x}) := \sum_{a=1}^{N^q} \phi_{,ij}^{(q,a)}(\mathbf{x}), \quad s_{ijk}(\mathbf{x}) := \sum_{a=1}^{N^q} \phi_{,ijk}^{(q,a)}(\mathbf{x}) \tag{18}$$

and adopting the modifications

$$\phi^{(q,a)}(\mathbf{x}) \to \tilde{\phi}^{(q,a)}(\mathbf{x}) := \phi^{(q,a)}(\mathbf{x})/s(\mathbf{x}), \quad \phi^{(q,a)}_{,i}(\mathbf{x}) \to \tilde{\phi}^{(q,a)}_{,i}(\mathbf{x}) := \phi^{(q,a)}_{,i}(\mathbf{x}) - s_i(\mathbf{x})\tilde{\phi}^{(q,a)}(\mathbf{x}),$$
$$\phi^{(q,a)}_{,ij}(\mathbf{x}) \to \tilde{\phi}^{(q,a)}_{,ij}(\mathbf{x}) := \phi^{(q,a)}_{,ij}(\mathbf{x}) - s_{ij}(\mathbf{x})\tilde{\phi}^{(q,a)}(\mathbf{x}), \quad \phi^{(q,a)}_{,ijk}(\mathbf{x}) \to \tilde{\phi}^{(q,a)}_{,ijk}(\mathbf{x}) := \phi^{(q,a)}_{,ijk}(\mathbf{x}) - s_{ijk}(\mathbf{x})\tilde{\phi}^{(q,a)}(\mathbf{x}) \tag{19}$$

one can guarantee satisfaction of the following equations

$$\sum_{a=1}^{N^q} \phi^{(q,a)}(\mathbf{x}) = 1 \ , \ \sum_{a=1}^{N^q} \phi^{(q,a)}_{,i}(\mathbf{x}) = 0 \ , \ \sum_{a=1}^{N^q} \phi^{(q,a)}_{,ij}(\mathbf{x}) = 0 \ , \ \sum_{a=1}^{N^q} \phi^{(q,a)}_{,ijk}(\mathbf{x}) = 0 \tag{20}$$

with the wave notation being omitted in the last equation. The formulation with using the standard shape functions will be denoted as S0-approach in contrast to S1-approach utilizing the modified shape functions.

3.2 Modified differentiation for approximation of derivatives of field variables

Moving Least Square (MLS) approximation

Besides the standard differentiation approach (denoted as "D0") we shall use also modified differentiation (denoted as D1-approach) in calculation of derivatives of field variables. In this approach, the derivatives are approximated by using the shape functions $\phi^a(\mathbf{x})$ and certain nodal values which will be expressed in terms of nodal values $\hat{u}^{\bar{h}}$ and the first order derivatives of the shape functions. Thus,

$$u_{,i}(\mathbf{x}) \approx \sum_{a=1}^{N^q} \hat{u}_i^{\bar{a}} \phi^{(q,a)}(\mathbf{x}) \ , \quad u_{,ij}(\mathbf{x}) \approx \sum_{a=1}^{N^q} \hat{u}_{ij}^{\bar{a}} \phi^{(q,a)}(\mathbf{x}) \ , \quad u_{,ijk}(\mathbf{x}) \approx \sum_{a=1}^{N^q} \hat{u}_{ijk}^{\bar{a}} \phi^{(q,a)}(\mathbf{x}) \ . \tag{21}$$

from (15_1), we have

$$u_{,i}(\mathbf{x}^c) \approx \sum_{h=1}^{N^c} \hat{u}^{\bar{h}} \phi^{(c,h)}_{,i}(\mathbf{x}^c) = \sum_{h=1}^{N^c} f_i^{ch} \hat{u}^{\bar{h}} \ , \text{ with } \ \bar{h} = n(c,h), \ f_i^{ch} = \phi^{(c,h)}_{,i}(\mathbf{x}^c) \tag{22}$$

while from (21_1), we have

$$u_{,i}(\mathbf{x}^c) \approx \sum_{a=1}^{N^c} \hat{u}_i^{\bar{a}} \phi^{(c,a)}(\mathbf{x}^c) = \sum_{h=1}^{N^c} e^{ca} \hat{u}_i^{\bar{a}} \ , \text{ with } \bar{a} = n(c,a), \ e^{ca} = \phi^{(c,a)}(\mathbf{x}^c). \tag{23}$$

Extending the definitions of matrices f_i^{ch} and e^{ca} to all nodes as

$$E^{cd} := \begin{cases} e^{ca}, d = \bar{a} \\ 0 \ , \ d \neq \bar{a} \end{cases} \ , \quad F_i^{cg} := \begin{cases} f_i^{ca}, g = \bar{a} \\ 0 \ , \ g \neq \bar{a} \end{cases} \ , \text{ with } \bar{a} = n(c,a), \ a \in \{1,2,...,N^c\} \ , \tag{24}$$

we can rewrite Eqs. (22) and (23) as

$$u_{,i}(\mathbf{x}^c) = \sum_{d=1}^{N} E^{cd}\hat{u}_i^d = \sum_{g=1}^{N} F_i^{cg}\hat{u}^g \ ,$$

hence,

$$\hat{u}_i^d = \sum_{g=1}^{N}\sum_{c=1}^{N}(E^{-1})^{dc}F_i^{cg}\hat{u}^g = \sum_{g=1}^{N} G_i^{dg}\hat{u}^g \quad , \quad G_i^{dg} := \sum_{c=1}^{N}(E^{-1})^{dc}F_i^{cg} \ . \tag{25}$$

Differentiating (21_1), we obtain

$$u_{,ij}(\mathbf{x}) \approx \sum_{a=1}^{N^q} \hat{u}_i^{\bar{a}}\phi_{,j}^{(q,a)}(\mathbf{x}) \ \Rightarrow \ u_{,ij}(\mathbf{x}^c) \approx \sum_{a=1}^{N^c} \hat{u}_i^{\bar{a}}\phi_{,j}^{(c,a)}(\mathbf{x}^c) = \sum_{g=1}^{N} F_j^{cg}\hat{u}_i^g \ . \tag{26}$$

From (21_2), we have

$$u_{,ij}(\mathbf{x}^c) \approx \sum_{a=1}^{N^c} \hat{u}_{ij}^{\bar{a}}\phi^{(c,a)}(\mathbf{x}^c) = \sum_{d=1}^{N} E^{cd}\hat{u}_{ij}^d \tag{27}$$

and from comparison of (26) with (27), we receive

$$\hat{u}_{ij}^d = \sum_{g=1}^{N}\sum_{c=1}^{N}(E^{-1})^{dc}F_j^{cg}\hat{u}_i^g = \sum_{g=1}^{N} G_j^{dg}\hat{u}_i^g = \sum_{g,h=1}^{N} G_j^{dg}G_i^{gh}\hat{u}^h \ , \tag{28}$$

where in the last equality, we have utilized the expression for $\hat{u}_i^g$ by (25)

Similarly,

$$\hat{u}_{ijk}^d = \sum_{g,b,h=1}^{N} G_k^{dg}G_j^{gb}G_i^{bh}\hat{u}^h \ . \tag{29}$$

Thus, having the expressions of $\hat{u}_i^d$, $\hat{u}_{ij}^d$, $\hat{u}_{ijk}^d$ by Eqs. (25), (28) and (29), one can utilize (21) for modified representation of derivatives of field variables in terms of shape function $\phi^{\bar{a}}(\mathbf{x})$ and all nodal values $\hat{u}^h$. In this approach (D1), only the first order derivatives at nodal points are employed in contrast to the standard approach (D0). Since inversion of the matrix E^{cd} is needed in evaluation of the matrix G_i^{dg} defined by (25), the lower computational efficiency of the D1-approach as compared with the D0-approach is the price which should be paid for a better accuracy of the D1-approach.

Point interpolation method (RBF+P)

In the modified differentation-approach (D1),

$$u_{,i}(\mathbf{x}) \approx \sum_{a=1}^{N^q} u_i^{\bar{a}}\varphi^{(q,a)}(\mathbf{x}) \ \Rightarrow \ u_{,i}(\mathbf{x}^c) \approx \sum_{a=1}^{N^c} u_i^{\bar{a}}\varphi^{(c,a)}(\mathbf{x}^c) = \sum_{a=1}^{N^c} u_i^{\bar{a}}\delta_{c\bar{a}} = u_i^c \tag{30}$$

we can see that the expansion coefficients u_i^c are directly given by the nodal values of the gradients of the field variable, which can be obtained from the D0-approach by

$$u_i^c = u_{,i}(\mathbf{x}^c) \approx \sum_{a=1}^{N^c} u^{\bar{a}} \varphi_{,i}^{(c,a)}(\mathbf{x}^c) = \sum_{a=1}^{N^c} f_i^{ca} u^{\bar{a}} \ , \quad \text{with} \quad f_i^{ca} := \varphi_{,i}^{(c,a)}(\mathbf{x}^c) \tag{31}$$

for higher order derivatives, we are seeking for the expressions

$$u_{,ij}(\mathbf{x}) \approx \sum_{a=1}^{N^q} u_{ij}^{\bar{a}} \varphi^{(q,a)}(\mathbf{x}) \ , \qquad u_{,ijk}(\mathbf{x}) \approx \sum_{a=1}^{N^q} u_{ijk}^{\bar{a}} \varphi^{(q,a)}(\mathbf{x}) \, . \tag{32}$$

hence,

$$u_{ij}^c = u_{,ij}(\mathbf{x}^c) \ , \quad u_{ijk}^c = u_{,ijk}(\mathbf{x}^c) \, . \tag{33}$$

Having known u_i^c, one can get the expression for $u_{,ij}(\mathbf{x})$ by differentiating (26_1)

$$u_{,ij}(\mathbf{x}) \approx \sum_{a=1}^{N^q} u_i^{\bar{a}} \varphi_{,j}^{(q,a)}(\mathbf{x}) \quad \Rightarrow \quad u_{ij}^c = u_{,ij}(\mathbf{x}^c) \approx \sum_{a=1}^{N^c} f_j^{ca} u_i^{\bar{a}} = \sum_{a=1}^{N^c} f_j^{ca} \sum_{g=1}^{N^{\bar{a}}} f_i^{\bar{a}g} u^{\bar{g}} \ , \tag{34}$$

where we have utilized also Eq. (33_1) and (31).

Similarly, differentiating (32_1) and using (33_2), (34_2), one obtains

$$u_{,ijk}(\mathbf{x}) \approx \sum_{a=1}^{N^q} u_{ij}^{\bar{a}} \varphi_{,k}^{(q,a)}(\mathbf{x}) \quad \Rightarrow \quad u_{ijk}^c = u_{,ijk}(\mathbf{x}^c) \approx \sum_{a=1}^{N^c} f_k^{ca} u_{ij}^{\bar{a}} = \sum_{a=1}^{N^c} f_k^{ca} \sum_{g=1}^{N^{\bar{a}}} f_j^{\bar{a}g} \sum_{h=1}^{N^{\bar{g}}} f_i^{\bar{g}h} u^{\bar{h}} \ . \tag{35}$$

Thus, making use of the Eqs. (31), (34_2) and (35_2), one can express the expansion coefficients u_i^c , u_{ij}^c , u_{ijk}^c in terms of nodal values u^a and the matrix of first order derivatives of the shape functions. Finally, the approximation formulae (30_1) and (32) are applicable and the higher order derivatives of the shape functions are avoided. In comparison with the MLS-approximation, the decrease of the efficiency of the numerical computations due to utilization of D1-approach is less expressive, since it is sufficient to pre-compute only the matrix f_i^{cg} instead of matrices E^{cd}, $(E^{-1})^{dc}$, F_i^{cg}.

Remark

Since the evaluation of the shape functions is a computational procedure, it is time consuming with substantial increasing the computational time with increasing the amount of such evaluations. Note that the evaluation of derivatives of shape function is much more time consuming than the evaluation of the shape functions especially in the case of modified differentiation approaches (D1) mainly for MLS –approximation. Furthermore, it is known that in weak formulations one needs to evaluate the integrands involving the shape functions and their derivatives at each integration point. Therefore a radical reduction of the evaluations of shape functions and their derivatives is achieved by using strong formulations instead of weak formulations. Thus, if the field variables are approximated by meshless approaches, the utilization of the strong formulation yields substantial

savings of the computational time in comparison with the weak formulations. This is an important aspect, because in case of sufficiently high density of nodal points used in approximation, the computational time needed for evaluation of the system matrix can exceed the computational time needed for solution of the discretized equations.

4. Numerical examples

In the numerical tests, we consider an annular circular plate with dimensionless inner radius $r_0 = 0.1$, outer radius $r_1 = 1$ and various gradations of the bending stiffness due to: (i) in-plane gradations of Young's modulus $E^*(r^*) = 1 + \varepsilon\left[(r^* - r_0^*)/(r_1^* - r_0^*)\right]^p$ and/or $E_1^*(r^*) = 1 + \varepsilon\left[(r_1^* - r^*)/(r_1^* - r_0^*)\right]^p$; (ii) in-plane continuous variation of the plate thickness $h^*(r^*) = 1 + \kappa\left[(r^* - r_0^*)/(r_1^* - r_0^*)\right]^s$; (iii) transversal gradation of Young's modulus $E^*(z) = 1 + \zeta\left(\frac{1}{2} + \frac{z}{h}\right)^p$; (iv) simultaneous radial gradations specified in points (i) and (ii). Poisson's ratio is assumed to be constant $\nu = 0.3$, while various values of the power-law gradation exponent (p) and levels of gradation (ε,κ,ζ) are considered. The dimensionless uniform static loading $\lambda_0^* = 1$ of plate is applied. Recall that it is no problem to find the exact solution for the boundary value problems if the bending stiffness is constant (Timoshenko, Woinowsky-Krieger, 1959; Sladek et al., 2013), but also for the governing equations if the bending stiffness is graded according to the power-law [Part I] as well as if the Young modulus is transversally graded according to the power-law [Part I]. Such exact solutions will be used as the benchmark solutions for investigation of the accuracy and convergence as well as computational efficiency of presented meshless method. The accuracy of numerical solutions of boundary value problems will be characterized by error norm defined as

$$\text{error norm} = 100\frac{\left(\sum_{a=1}^{N}\left\{\left[w(r^a) - w^{ex}(r^a)\right]^2 + \left[m(r^a) - m^{ex}(r^a)\right]^2\right\}\right)^{1/2}}{\left(\sum_{a=1}^{N}\left\{\left[w^{ex}(r^a)\right]^2 + \left[m^{ex}(r^a)\right]^2\right\}\right)^{1/2}}\ (\%) \tag{36}$$

where N is the total number of nodal points, $w(r^a)$ and $m(r^a)$ are the values of field variables computed by the present method, while $w^{ex}(r^a)$ and $m^{ex}(r^a)$ are exact values at nodal points r^a.

In all numerical computations, we have used a uniform distribution of nodal points and the radius of the sub-domain $\rho_0 = 0.1h$ with h being the distance between two neighbour nodes. The other parameters in the MLS-approximation have been taken as: radius of the interpolation domain $\rho^a = 3.001h$, shape function parameter $c^a = h$, cubic polynomial basis $m = 4$. In the PIM(RBF+P)-approximation, we have chosen: type of RBF – inverse multi-quadrics with $\mu = -1$, number of multi-quadrics around each node $N^q = 16$, number of polynomials $M = 7$, shape parameter $c^a = 2h$. As regards the geometry, we have considered the circular plate with central hole $\Omega = \{\forall(r,\varphi); r \in [r_0, r_1],\ \varphi \in [0, 2\pi]\}$.

Firstly, we present the results of the study of accuracy, convergence and computational efficiency. In presented results, both edges of the plate are clamped ($w(r_0) = 0$, $w_{,r}(r_0) = 0$; $w(r_1) = 0$, $w_{,r}(r_1) = 0$) because there is no principal difference among the results corresponding to other boundary conditions. The transversal variation of the dimensionless Young modulus is shown in Figure 1. The

accuracy and the convergence of the accuracy with respect to increasing the density of nodes (decreasing the h – parameter) are shown in Figures 2 – 3, with using the PIM and MLS approximations, respectively. It can be seen that the influence of S1-modification for evaluation of shape functions and their derivatives on accuracy is negligible. In FGM plates, the improvement of accuracy by the modified differentiation (D1-approach) as compared with the standard differentiation (D0-approach) is not guaranteed in contrast to the numerical computations for plates with constant bending stiffness (Sladek, Sladek and Sator, 2013), where the achieved accuracy is also several orders higher. Nevertheless, in case of the FGM plate with transversal gradation of Young's modulus by MLS approximation of field variables the accuracy improvement by D1-approach is increasing with increasing the density of nodes. On the other hand, in the case of FGM plates with radial gradation of the bending stiffness, the accuracy of MLS results by the D0-approach is better until rather high densities of nodes, though the convergence rate by the D1-approach is better than that by the D0--approach.

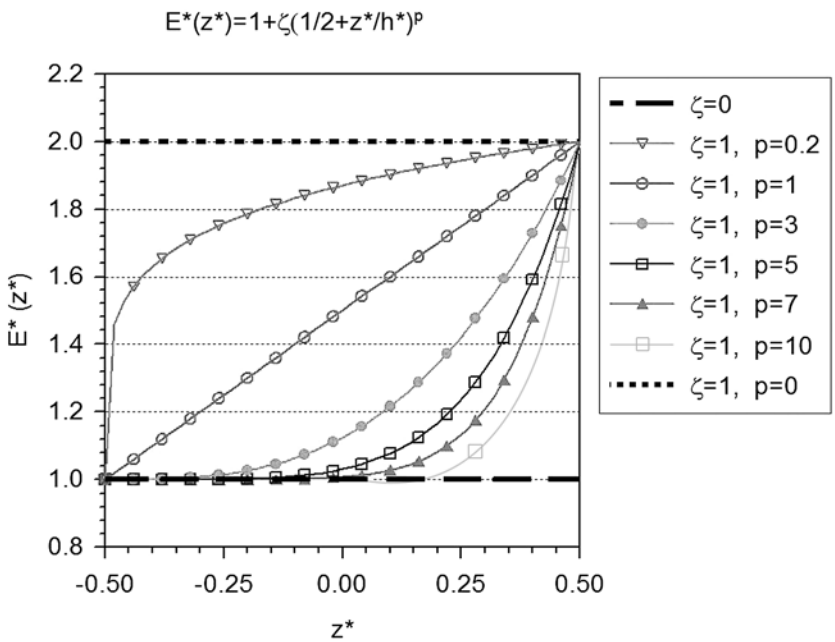

Figure 1. Illustration of the transversal gradations of the Young modulus across the plate thickness for several values of the exponent (p) of the power-law gradation with the level of gradation $\zeta = 1$

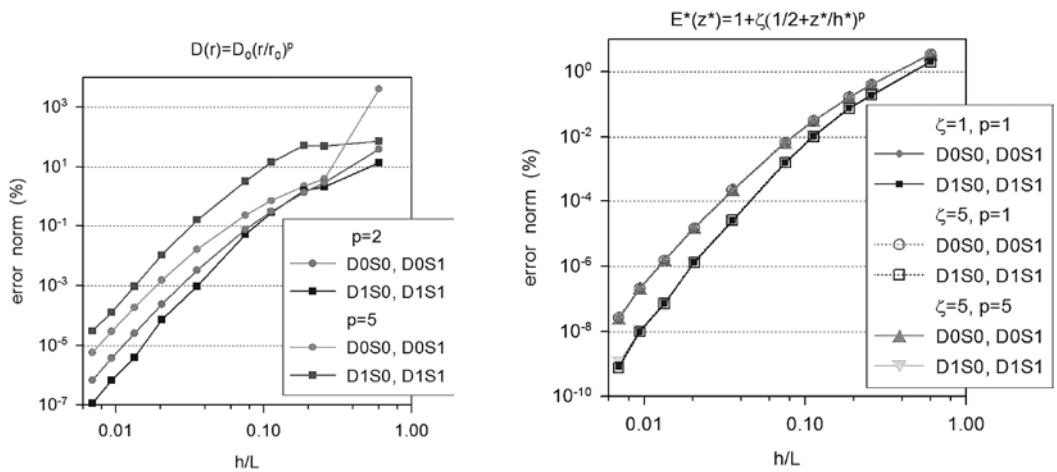

Figure 2. Accuracy and convergence of accuracy of numerical solutions for plate with (i) power--law radial gradation of bending stiffness; (ii) transversal gradation of Young's modulus by PIM approximation

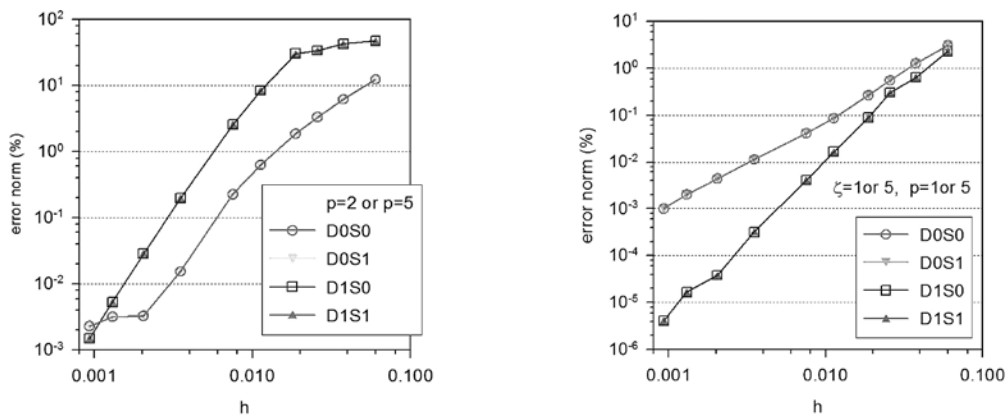

Figure 3. Accuracy and convergence of accuracy of numerical solutions for plate with (i) power--law radial gradation of bending stiffness; (ii) transversal gradation of Young's modulus by MLS approximation

From Figure 4, we can see that the computational times are almost invariable with respect to various gradation of bending stiffness. A substantial difference is observed for the rates of increasing the CPU with increasing the density of nodes when D0- and D1-approaches are used for evaluation of the 2nd order derivatives of field variables especially for large amounts of nodes. The utilization of the D1-approach brings a significant enhancement of the rate of the CPU-time increase. The prolongation of the CPU-time is due to more complex procedure for evaluation of the derivatives of field variables than in the case of D0-approach. The significant increase of the CPU-time appears to be an unacceptable price for improving the accuracy of numerical solutions by using D1-approach.

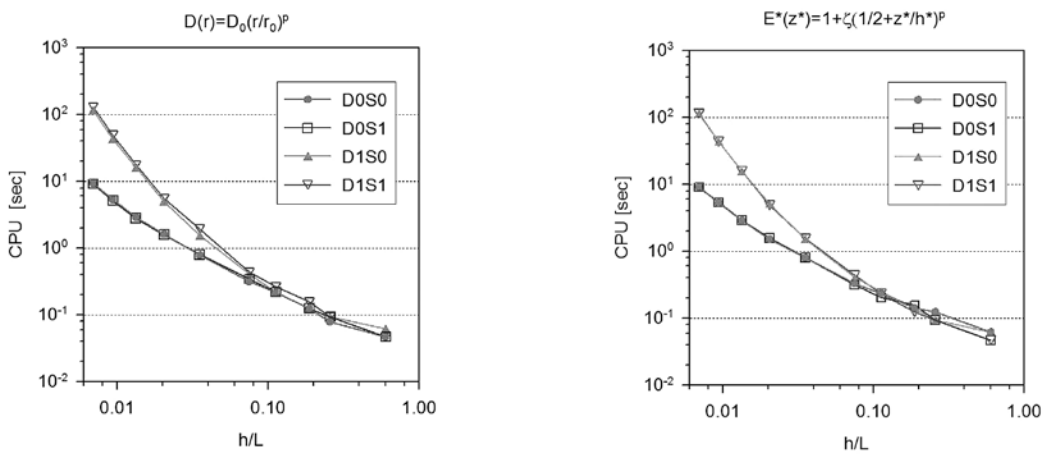

Figure 4. Computational efficiency of numerical solutions for plate with (i) power-law radial gradation of bending stiffness; (ii) transversal gradation of Young's modulus

4.1. Results for circular plate with transversal gradation of Young's modulus

In what follows, we shall present numerical results for a plate with transversal gradation of Young's modulus, with studying the influence of coupling effect (c-factor) between the deflections (w) and radial displacements (u_r); and the influence of the stress state conditions (χ-factor) on the solution:

- $c = 1 : w - u_r$ coupling is considered,
- $c = 0 : w - u_r$ coupling is omitted,
- $\chi = 1$: plane stress state formulation,
- $\chi = 2$: spatial stress state formulation.

Figure 5 illustrates the influence of gradation of Young's modulus on the reduction of deflections against the deflections of homogeneous plate, where with increasing the level of gradation the deflections of plate are decreasing. The results are presented for two levels of gradation (ζ) and various combinations of the c and χ-factors. The reduction of the deflection is increasing with increasing the level of gradation. The reduction of the maximum deflection is around 20 % lower in the case of plane stress formulation than in the case $\chi = 2$ with keeping the c-factor constant. This observation is independent on the value of the c-factor. In the case of higher level of gradation, the differences between the results corresponding to c=0 and c=1 under fixed value of the χ-factor are comparable with differences due to various values of the χ-factor under fixed value of the c-factor. Furthermore, the coincidence of results in formulations with (c=1, $\chi = 2$) and with (c=0, $\chi = 1$) for $\zeta = 5$ can be observed. Figure 6 shows the radial variations of radial displacements, which were generated by w—u_r coupling (c=1). The influences of ζ and χ-factor are observable. Eventually, we can conclude that the dimensionless bending moments (M^*_{rr}) are independent on the c and χ-factors (Fig. 7), in contrast to the dimensionless deflection (w*).

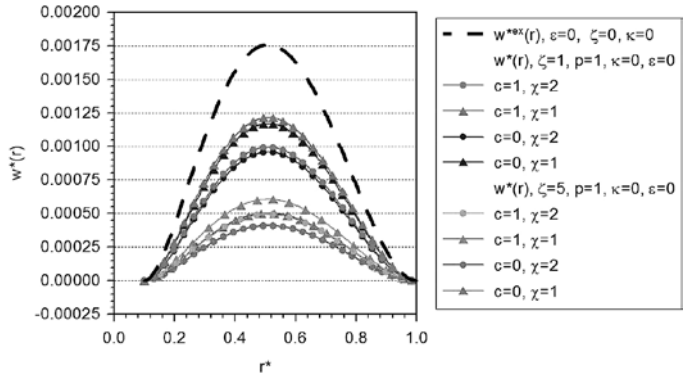

Figure 5. Radial distribution of deflections in circular plate with transversal gradation of the Young modulus

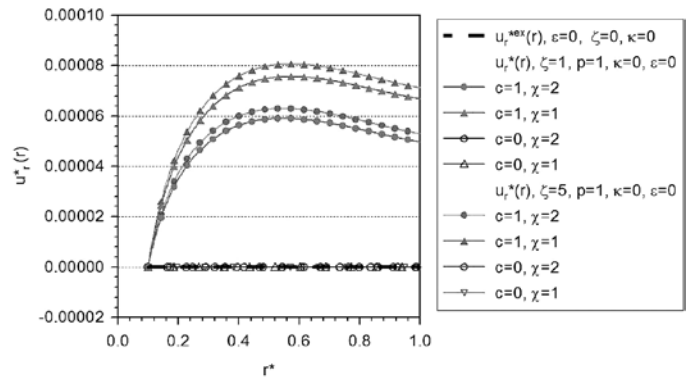

Figure 6. Distribution of radial displacements generated via coupling effect in circular plate with transversal gradation of the Young modulus

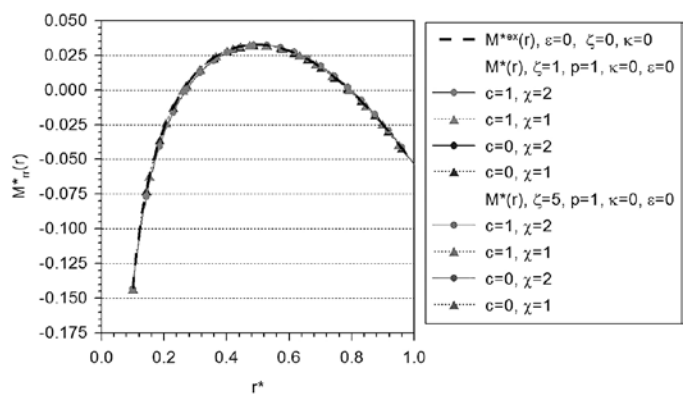

Figure 7. Distribution of bending moments in circular plate with transversal gradation of the Young's modulus

Figures 8 – 9 show the dependence of maximum value of deflection and/or reduction of maximum value of deflection on the parameter ζ (level of gradation) and exponent p (power-law exponent of gradation), respectively. In Figure 8 we can see that the maximum value of deflection is decreasing and/or reduction of the maximum value of deflection w.r.t. the $w^*_{ref} = w^*(\zeta = 0, \chi = 1)$ is increasing with increasing the level of gradation under keeping the volume contents of the constituents to be constant (p = const). Figure 9 shows the increasing maximum deflection and/or the decreasing reduction of the maximum deflection (due to the transversal gradation of Young's modulus) with increasing the value of the exponent of power-law gradation of Young's modulus. This can be explained by the fact that the volume content of the constituent with higher Young modulus is decreasing with increasing the exponent p.

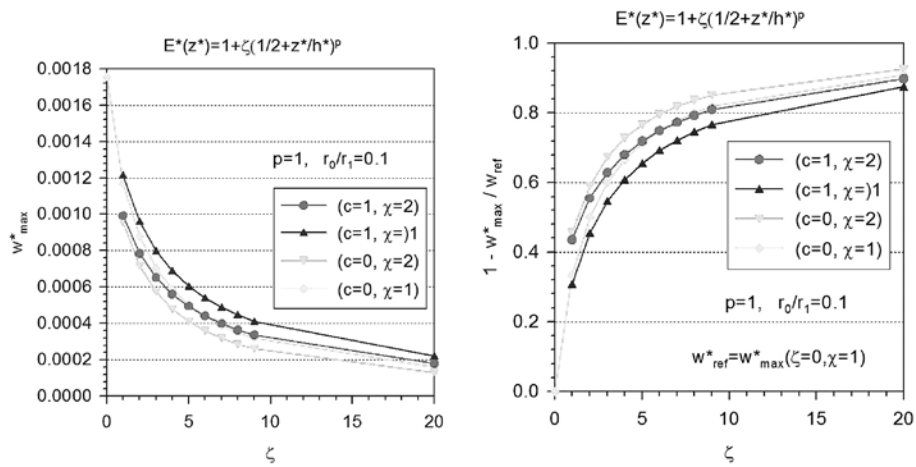

Figure 8. Dependence of (i) the maximum deflection and (ii) the reduction of the maximum deflection on level of gradation ζ

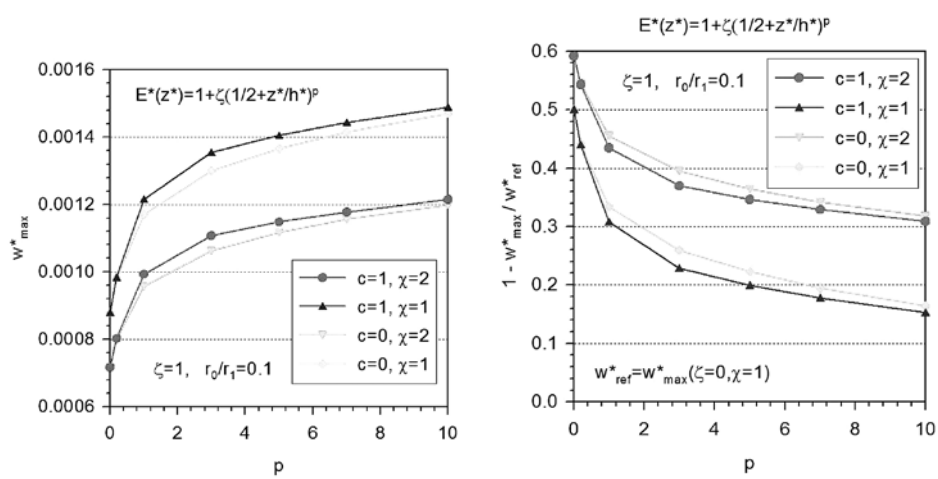

Figure 9. Dependence of (i) the maximum deflection and (ii) the reduction of the maximum deflection on power-law exponent of gradation p

Finally, we present the study of the dependence of percentage deviation of maximum deflection ($w^*_{\max}$) from the reference value of deflection ($w^*_{\text{ref}} = w^*_{\max}$ (c=1, χ=2). From Figure10, we can see that the deviation between the maximal dimensionless deflection and the reference value for low level of gradation ($\zeta = 1$) is approximately 4 %, while for the high level of gradation ($\zeta = 20$) this value is equal almost to 30%. Moreover, one can observe the influence of χ-factor, the 22.5 % difference between the results by the formulations with $\chi = 1$ and $\chi = 2$ under constant value of the *c*-factor.

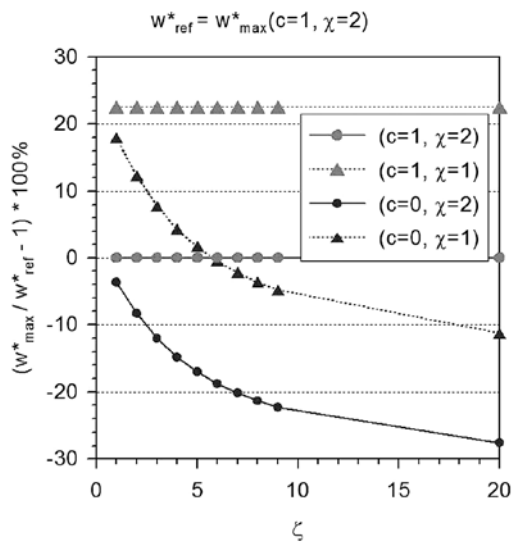

Figure 10. Dependence of % deviations of $w^*_{\max}$ from w^*_{ref} on ζ-parameter in FGM circular plate

4.2. Results for circular plate with gradation of Young's modulus in radial directions

In this subsection we shall present the results for the circular plate with central circular hole and power-law gradation of Young's modulus in the radial direction.

In what follows we concise to presentation of numerical results for deflections, slopes of deflections, bending moments and generalized shear forces in the considered boundary value problem and two values of gradation exponent (p = 1,5) and/or two levels of gradation (ε = 1,5). The significant influence of these parameters on the values as well as on the radial distributions of the considered fields is presented in Figures 11 – 15. In all computations, we consider two various kinds of gradation of Young's modulus: (i) gradation from the inner radius towards to the outer radius ($E^*(r^*) = 1 + \varepsilon[(r^* - r_0^*)/(r_1^* - r_0^*)]^p$); and (ii) gradation from the outer radius towards to inner radius ($E_1^*(r^*) = 1 + \varepsilon[(r_1^* - r^*)/(r_1^* - r_0^*)]^p$). Figure 11 illustrates that the higher value of parameter ε is leading to a higher reduction of maximum deflection under the constant contents of two material constituents. On the other hand, the higher value of the exponent p leads to a lower reduction of the maximum deflection (Fig. 12), what is the effect of lower bulk content of the material with higher value of the Young modulus.

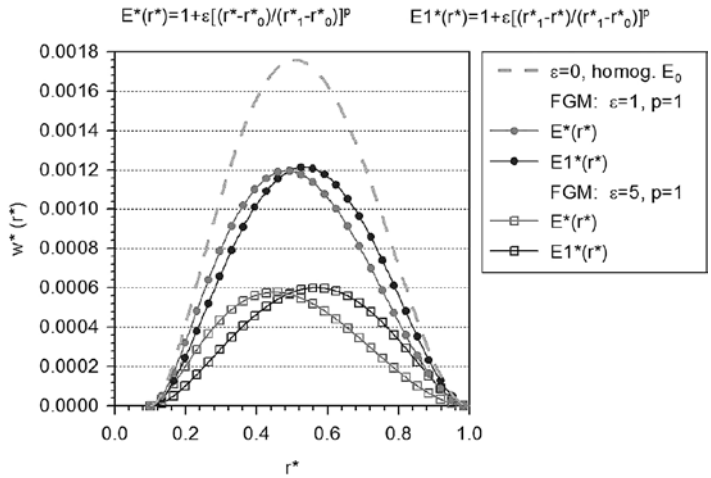

Figure 11. Comparison of the deflections of the circular plate for various levels of gradation ε and two kinds of gradation of Young's modulus

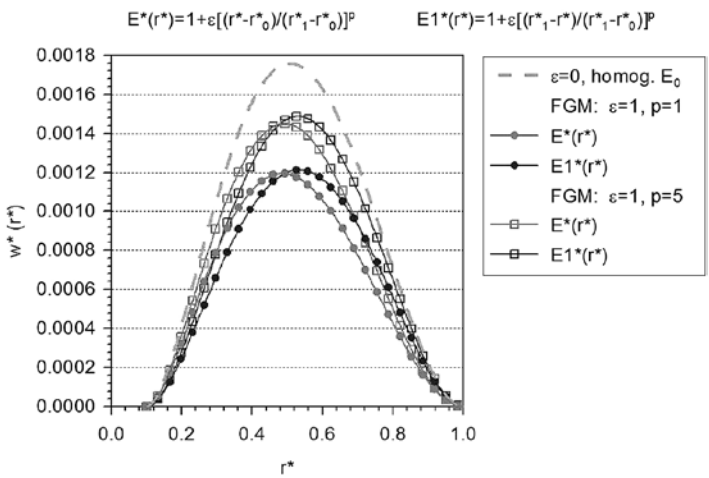

Figure 12. Comparison of the deflections of the circular plate for various gradation exponent *p* and two kinds of gradation of Young's modulus

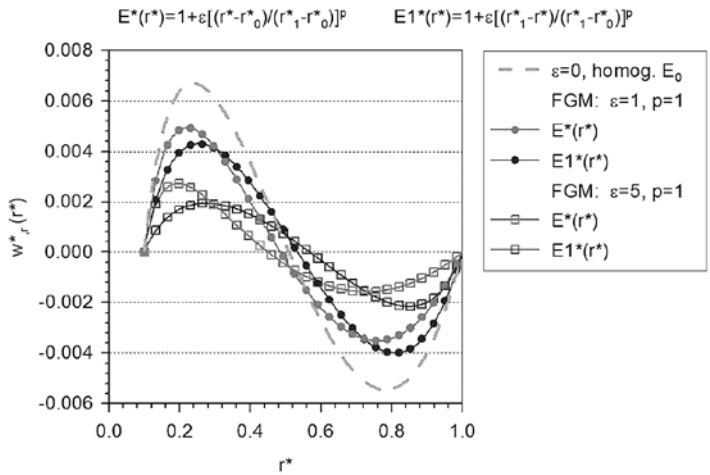

Figure 13. Comparison of the slopes of deflections of the circular plate for various levels of gradation ε and two kinds of gradation of Young's modulus

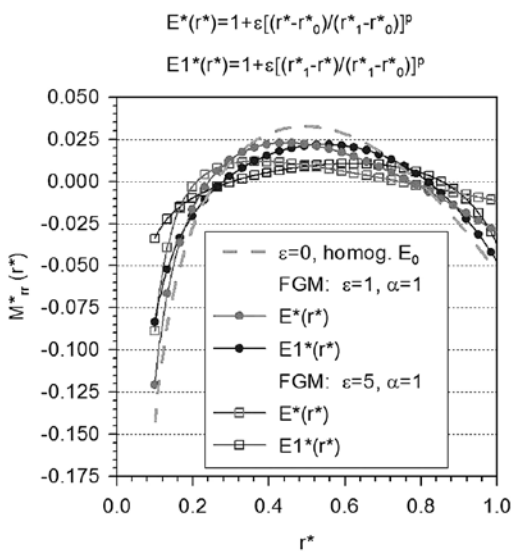

Figure 14. Comparison of the bending moments in the circular plate for various levels of gradation ε and two kinds of gradation of Young's modulus

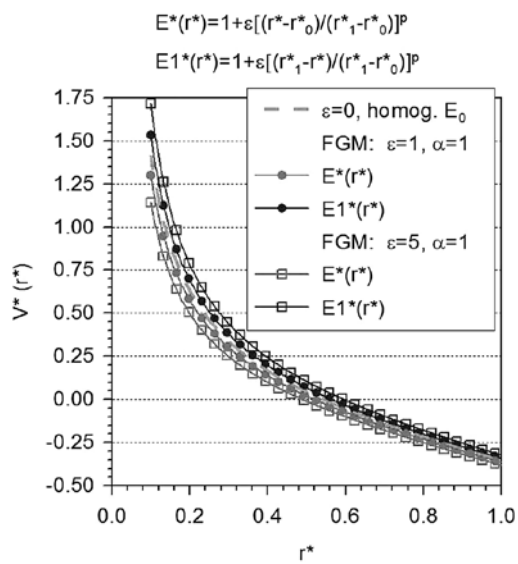

Figure 15. Comparison of the generalized shear forces in the circular plate for various levels of gradation ε and two kinds of gradation of Young's modulus

4.3. Results for circular plate with radial continuous variations of the plate thickness

Firstly, let us consider a circular plate with homogeneous material properties, while the thickness of the plate is varied by a power-law function. Numerical results for deflections, slopes of deflecti-

ons, bending moments and generalized shear forces for the considered thin plate and three levels of gradation ($\kappa = -0.5,1,2$) are presented in Figures 16 – 19. It can be observed that the reduction of thickness ($\kappa < 0$) yields enhancement of deflections, slopes of deflections, bending moments and generalized shear forces as compared with $h = const = h_0$. On the other hand, the increasing thickness ($\kappa > 0$) leads to reduction of physical quantities as compared with $h = const = h_0$. Finally, in Figures 16 – 19, we present also the comparison of effects on the results due to pure radial gradation of the Young modulus and pure gradation of the plate thickness. The latter effect is more expressive than the effect of variability of the Young modulus.

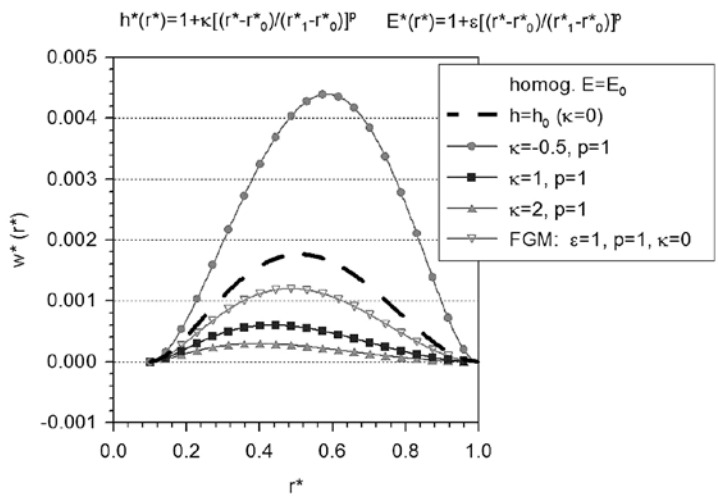

Figure 16. Comparison of the deflections of the circular plate for various levels of gradation κ of the plate thickness

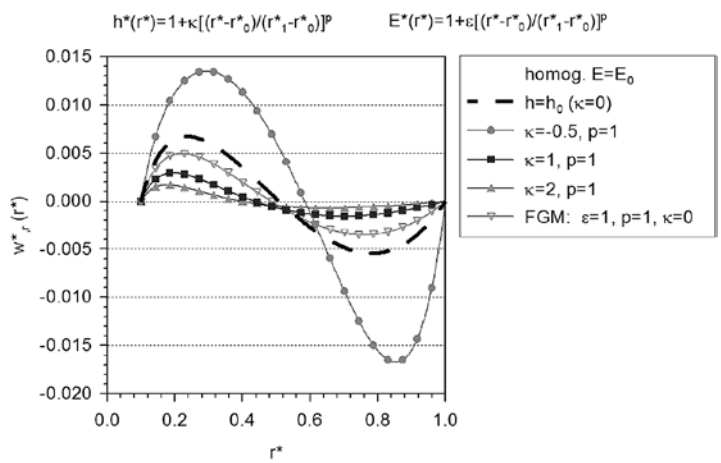

Figure 17. Comparison of the slopes of deflections of the circular plate for various levels of gradation κ of the plate thickness

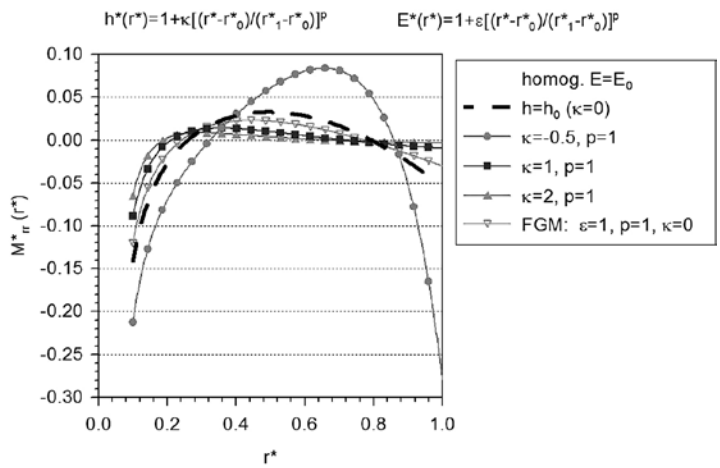

Figure 18. Comparison of the bending moments in the circular plate for various levels of gradation κ of the plate thickness

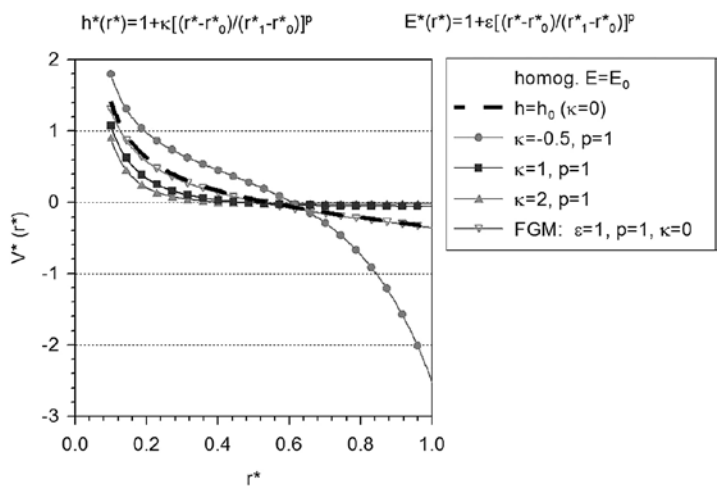

Figure 19. Comparison of the generalized shear forces in the circular plate for various levels of gradation κ of the plate thickness

Finally, we studied also simultaneous continuous radial variations of both the plate thickness and Young's modulus (Fig. 20). The negative effect of thinning the plate (blue line) can be compensated or suppressed by parallel gradual increasing the Young modulus (green line) with resulting in overall reduction of deflection (red line).

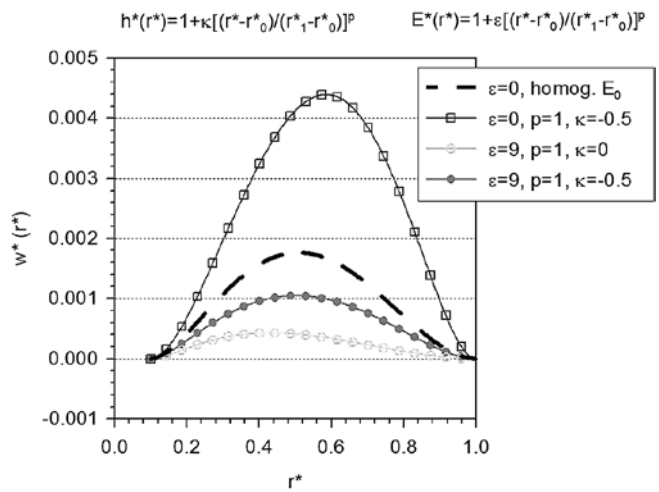

Figure 20. Illustration of positive effect of combination of the radial gradations of the plate thickness and the Young modulus

5. Conclusions

Bending of thin elastic plates with variable bending stiffness has been studied within Kirchhoff--Love theory. In the paper we consider several types of variability of bending stiffness due to:

(i) FGM: (a) in-plane gradation of Young's modulus,
(b) transversal gradation of Young's modulus;
(ii) variable thickness of plate;
(iii) simultaneous radial variations of the Young modulus and the plate thickness.

The strong meshless formulation has been developed for numerical solution of boundary value problems for plate bending with using two meshless approximations such as the MLS-approximation and the PIM (RBF+PBF). The problem of high-order derivatives of field variables has been resolved by the development of decomposed formulation of governing equations.

The convergence of proposed computational schemes has been studied with using two approaches for evaluation of derivatives of field variables and two approaches for evaluation of shape functions. The comparative study for computational efficiency of various techniques has been accomplished. Numerical experiments have been done for study of the influence of bending stiffness variability on response of the plate subjected to static loading with focusing on the coupling effects and effect of the plane stress formulation.

Acknowledgements

The financial support by APVV-0032-10 (Slovak Research and Development Agency) is greatly acknowledged.

REFERENCES

[1] Atluri, S. N. (2004), The Meshless Method, (MLPG) For Domain & BIE Discretizations, Tech Science Press, Encino.

[2] Benveniste, Y. (1987), A new approach to the application of Mori-Tanaka's theory in composite materials. Mech Mater 6, 147-157.

[3] Chamis, C. C. and Sendeckyj, G. P. (1968), "Critique on theories predicting thermoelastic properties of fibrous composites", J Compos Mater 2, 3:332-358.

[4] Gibson, R. F. (1994), Principles of composite material mechanics. McGraw-Hill.

[5] Hashin, Z. and Rosen, B. W. (1964) "The elastic moduli of fiber-reinforced materials", ASME J Appl Mech 4, 223-232.

[6] Hashin, Z. (1979), "Analysis of properties of fiber composites with anisotropic constituents", ASME J Appl Mech 46, 543-550.

[7] Koizumi, M. (1997), FGM activities in Japan. Composites Part B 28, 1-4.

[8] Krysl, P. and Belytschko, T. (1995), Analysis of thin plates by the element-free Galerkin method, Computational Mechanics 17, 26-35.

[9] Lancaster, P. and Salkauskas, K. (1981), Surfaces generated by moving least square method, Mathematics of Computations 37, 141-158.

[10] Liu, G. R. (2003), Mesh Free Methods, Moving Beyond the Finite Element Method, CRC Press: Boca Raton.

[11] Lu, Y.Y., Belytschko, T. and Gu, L. (1994), A new implementation of the element free Galerkin method, Comp. Meth. Appl. Mech. Eng. 113, 397-414.

[12] Mori, T. and Tanaka, T. (1973) Average stress in matrix and average elastic energy of materials with misfitting inclusions, Acta Metall 21, 571-574.

[13] Sladek, V., Sladek, J. and Tanaka, M. (2005), Local integral equations and two meshelss interpolations with application to potential problems in non-homogeneous media, CMES-Comp. Model. Eng. Sci. 7, 69-83.

[14] Sladek, V., Sladek, J. and Zhang, Ch. (2008) Computation of stresses in non-homogeneous elastic solids by local integral equation method: a comparative study, Comput. Mech. 41, 827-845.

[15] Sladek, V., Sladek, J. and Zhang, Ch. (2008) Local integral equation formulation for axially symmetric problems involving elastic FGM, Engineering Analysis with Boundary Elements 32,1012-1024.

[16] Sladek, V. and Sladek, J. (2010), Local integral equations implemented by MLS approximation and analytical integrations, Engineering Analysis with Boundary Elements 34, 904-913.

[17] Sladek, V., Sladek, J. and Sator, L. (2013), Physical decomposition of thin plate bending problems and their solution by mesh-free methods, Engineering Analysis with Boundary Elements 37, 348-365.

[18] Suresh, S. and Mortensen, A. (1998), Fundamentals of functionally graded materials, 1st ed. London: IOM Communications.

[19] Reddy, J. N., Wang, C. M. and Kitipornchai, S. (1999), "Axisymmetric bending of functionally graded circular and annular plates", Eur j Mech A/Solids 18, 185-199.

[20] Reddy, J. N. (2000), "Analysis of functionally graded plates", Int J Numer Meth Eng 47, 663-684.

[21] Xu, Y. and Zhou, D. (2009), Three-dimensional elasticity solution of functionally graded rectangular plates with variable thickness, Composite Structures 91, 1:56-65.